

A simple raster-based model for flood inundation simulation

P.D. Bates^{a,*}, A.P.J. De Roo^{b,1}

^aResearch Centre for Environmental and Geophysical Flows, School of Geographical Sciences, University of Bristol, Bristol, BS8 1SS, UK

^bNatural Hazards Project, ARIS Unit, Space Applications Institute, European Commission Joint Research Centre, T.P. 262, 21020 Ispra (VA) Italy

Received 4 November 1999; revised 31 March 2000; accepted 17 May 2000

Abstract

In this paper the development of a new model for simulating flood inundation is outlined. The model is designed to operate with high-resolution raster Digital Elevation Models, which are becoming increasingly available for many lowland floodplain rivers and is based on what we hypothesise to be the simplest possible process representation capable of simulating dynamic flood inundation. This consists of a one-dimensional kinematic wave approximation for channel flow solved using an explicit finite difference scheme and a two-dimensional diffusion wave representation of floodplain flow. The model is applied to a 35 km reach of the River Meuse in The Netherlands using only published data sources and used to simulate a large flood event that occurred in January 1995. This event was chosen as air photo and Synthetic Aperture Radar (SAR) data for flood inundation extent are available to enable rigorous validation of the developed model. 100, 50 and 25 m resolution models were constructed and compared to two other inundation prediction techniques: a planar approximation to the free surface and a relatively coarse resolution two-dimensional finite element scheme. The model developed in this paper outperforms both the simpler and more complex process representations, with the best fit simulation correctly predicting 81.9% of inundated and non-inundated areas. This compares with 69.5% for the best fit planar surface and 63.8% for the best fit finite element code. However, when applied solely to the 7 km of river below the upstream gauging station at Borgharen the planar model performs almost as well (83.7% correct) as the raster model (85.5% correct). This is due to the proximity of the gauge, which acts as a control point for construction of the planar surface and the fact that here low-lying areas of the floodplain are hydraulically connected to the channel. Importantly though it is impossible to generalise such application rules and thus we cannot specify a priori where the planar approximation will work. Simulations also indicate that, for this event at least, dynamic effects are relatively unimportant for prediction of peak inundation. Lastly, consideration of errors in typically available gauging station and inundation extent data shows the raster-based model to be close to the current prediction limit for this class of problem. © 2000 Elsevier Science B.V. All rights reserved.

Keywords: Floodplains; Floodplain inundation; Hydraulic modelling; Synthetic aperture radar

1. Introduction

Estimation of reach scale flood inundation is increasingly a major task for river engineers and managers (see Penning-Rowsell and Tunstall, 1996). For most rivers sufficient observations of flood inundation extent are not available to determine such areas

* Corresponding author. Tel.: +44-117-928-9108; fax: +44-117-928-7878.

E-mail addresses: paul.bates@bristol.ac.uk (P.D. Bates), ad.de-roo@jrc.it (A.P.J. De Roo).

¹ Tel.: +39-033-278-6240; fax: +39-033-278-5500.

and recourse must be made to some sort of predictive 'model'. These can range in complexity from simply intersecting a plane representing the water surface with a Digital Elevation Model (DEM) of sufficient resolution to give the flooded area (see for example Priestnall et al., 2000) to full three-dimensional solutions of the Navier–Stokes equations with sophisticated turbulence closure (see for example Thomas and Williams, 1995; Younis, 1996). However, prediction of flood inundation is not straightforward. Out-of-bank flow in meandering compound channels is now known to be highly three-dimensional and involves the development of a strong shear layer between main channel and floodplain (Knight and Shiono, 1996) as well as spillage of water from the main channel across meander loops (Ervin et al., 1993; Ervin et al., 1994; Sellin and Willets, 1996). Moreover, flood inundation extent is highly dependent on topography, and shallow floodplain gradients mean that small errors in modelled water surface elevations may lead to large errors in the predicted inundation front position.

At present we still do not know what process representation it is necessary to include in a floodplain inundation model to achieve given levels of predictive ability. Ultimately, the best model will be the simplest one that provides the information required by the user whilst reasonably fitting the available data. However, modellers tend to employ the most sophisticated scheme that can be practically applied in the belief that the more processes a model includes the better it will be. Whilst this may be a reasonable assumption, it has never been tested for the specific task of predicting flood inundation.

For example, until relatively recently the most popular approaches to modelling fluvial hydraulics, and thus implicitly flood inundation, at the reach scale (5–50 km) have been one-dimensional finite difference solutions of the full St. Venant equations (see for example Fread, 1984; Samuels, 1990; Fread, 1993; Ervin and MacLeod, 1999) such as MIKE11, ISIS, ONDA, FLUCOMP and HEC-RAS. Such schemes describe the river channel and floodplain as a series of cross sections perpendicular to the flow direction and are thus well suited to parametrisation using traditional field surveying methods. Numerical solution of the controlling equations for prescribed inflow and outflow boundary conditions then enables

the cross section-averaged velocity and water depth at each location to be calculated. However, considerable skill is required to determine appropriate cross section locations for such models (Samuels, 1990) and, in addition, areas between cross sections are not explicitly represented. To simulate flood inundation extent the values of water depth at each cross-section are taken and either overlain onto a DEM or the inundation extents at each cross section are linearly interpolated. To overcome these limitations, two-dimensional finite difference and finite element models have been developed (see for example Feldhaus et al., 1992; Bates et al., 1992; Bates et al., 1995). These provide a higher order representation of river hydraulics more consistent with known processes, include a continuous representation of topography and require no secondary processing step to determine the flood inundation. Recently, such schemes have been compared successfully to low resolution satellite imagery of flood inundation extent (Bates et al., 1997) and measured water levels internal to the model domain during dynamic simulations (Bates et al., 1998). However, they have the drawback of increased computational cost and are less well suited to parametrisation with traditional cross sectional surveys. Two-dimensional models are best employed in conjunction with a DEM of the channel and floodplain surface that, in conjunction with suitable inflow and outflow boundary conditions, allows the water depth and depth-averaged velocity to be computed at each computational node at each time step. Thus the sophistication of flood inundation modelling has increased in line with model developments and increased computational resources, but the possibility that simpler models may provide similar levels of predictive ability has not actually been considered.

A further impetus for such a development is the increasing availability of high resolution, high accuracy Digital Elevation Models for floodplain areas. National topographic mapping agencies have tended to treat low-lying floodplain areas as relatively featureless. This lack of data has been addressed in a number of countries (UK, The Netherlands) using techniques such as aerial photogrammetry and airborne laser altimetry (Li, 1997), both of which are capable of rapidly generating high resolution DEMs. Large amounts of digital elevation data are now being generated by such programmes and there

is a need for hydraulic schemes that are able to directly capture as much of this information content as possible and from it generate inundation extent predictions. Two-dimensional numerical models are a possibility here as they can be readily integrated with such data sources (see Marks and Bates, 2000); however, for the reasons given above and the quantity of data and the number of reaches involved, the availability of simpler modelling tools would also be beneficial. These should ideally be capable of being used by environmental managers with relatively little hydraulic modelling experience.

This then is the focus of the paper, where we describe the development and testing of a simple physically-based flood inundation model, LISFLOOD-FP, capable of being integrated with newly available high resolution raster-based Digital Elevation Models. This new scheme is an extension of the LISFLOOD catchment model (De Roo et al., 1999a) and is specifically designed for channel and floodplain hydraulic routing problems. It aims to reduce the representation of floodplain hydraulics to the minimum necessary to achieve acceptable predictions when compared to typically available flood hydraulic data. At best this consists of gauged discharge and stage records and satellite and air photo derived flood extent data, with simulation of the latter being the primary focus of the scheme. Flow velocity is not generally collected by environmental authorities and is not specifically required by most statutory flood risk regulations. It can, for the purposes of flood inundation prediction, be considered as a 'redundant' variable and for this reason is not explicitly considered by the model. Finally, the new scheme is simple to set up and run, computationally efficient, can be used by non-expert users and can be readily integrated with commercial Geographic Information Systems.

2. LISFLOOD-FP model development

The basic component of the LISFLOOD-FP model is a raster Digital Elevation Model of resolution and accuracy sufficient to identify both the channel (location and slope) and those elements of the floodplain topography (dykes, embankments, depressions and former channels) considered necessary to flood inun-

dation prediction. In reality this resolution and accuracy cannot be known a priori and may vary between applications, so an informed guess is needed as a starting point for model development. In time, we should be able to determine guidelines for this aspect of the model development process.

Having defined our basic data source the next step is to consider the process representation we need to include. A flood consists of a large, low amplitude wave propagating downvalley. When the bankfull flow depth is reached, water ceases to be contained solely in the main river channel and water spills onto adjacent shallow gradient floodplains. These floodplains act either as temporary stores for this water or additional routes for flow conveyance. For channel flow below bankfull depth there is increasingly a consensus (Knight and Shiono, 1996) that flow processes can be represented by a simple one-dimensional representation. For the out-bank case this situation is more complex. Floodplain flow is clearly two-dimensional, whilst at the channel–floodplain interface development of intense shear layers leads to a strongly turbulent and three-dimensional flow field (see for example Tominaga and Nezu, 1991; Sellin and Willetts, 1996). Again, it is therefore difficult to make a priori decisions about which processes it is necessary to include in a flood inundation model. However, we might begin by assuming that because of the process complexity schemes that fail to capture dynamic flood wave behaviour, such as the planar surface model described in Section 1, will be poor predictors of inundation extent. At its most basic level this is because floods are not planar surfaces but, rather, are waves where the shape of the wave (or hydrograph as it would appear to a stationary observer) will control the rate of floodplain wetting and drying. Perhaps more importantly, the planar surface assumption can result in areas being flooded that are never connected to the flood. As a working hypothesis we therefore take as our starting point the minimum process representation capable of dynamic simulations. This consists of a one-dimensional hydraulic routing procedure for channel flow to capture the downstream propagation of the flood wave and some distributed means of routing water two-dimensionally over the floodplain to enable simulation of floodplain water depths and hence inundation extent. Ideally, some account of the interaction

between main channel and floodplain could also be made; however, this is not an essential part of the minimum specification but rather a possible later refinement. The most basic dynamic wave routing scheme available consists of the kinematic wave approximation. This is a simplification of the full one-dimensional St. Venant equation obtained by eliminating local acceleration, convective acceleration and pressure terms in the momentum equation. It thus assumes that the friction and gravity forces balance (see Singh, 1996 for an extensive treatment). The resulting equation system is therefore:

- Continuity

$$\frac{\partial Q}{\partial x} + \frac{\partial A}{\partial t} + q = 0 \quad (1)$$

- Momentum

$$S_0 = S_f \quad (2)$$

where Q is the discharge [L^3T^{-1}], x is the distance between cross sections [L], A is the flow cross sectional area [L^2], t is the time [T], q is a lateral inflow term [L^3T^{-1}] here set to zero for all reported simulations, S_0 is the channel bed slope [$-$] and S_f is the friction slope [$-$] here approximated as the water surface slope.

Given two channel cross sections Δx apart the above equations can be solved numerically to yield the discharge, Q , and flow cross sectional area A , and hence the water depth. The simplest numerical solution of the above equation system is an explicit finite difference procedure. A number of such schemes are available and we here implement the one given by Chow et al. (1988). This is a simple linear scheme that uses the backward-difference method to derive the finite difference equations. The reader is referred to Chow et al. (1988) for a complete description of this method. The limitations of Eq. (2) are that only down gradient characteristics of the hydraulics are considered, backwater effects are ignored and there is a possibility of shock waves developing in areas of flow convergence.

To implement the kinematic routing model we define a local drainage direction map that represents the line of the channel. Commencing at the

inflow point each channel cell contains a marker indicating the direction of the next downstream channel cell. For each cell containing a channel we define the channel width, slope, friction coefficient and bankful depth. Hence the cross-sectional geometry is assumed to be rectangular. Whilst the channel width may be greater or smaller than the resolution of the raster DEM to give flexibility in the channel representation, these dimensions should not vary too greatly to avoid undue approximation errors. For each channel cell we therefore have all the necessary information to compute the kinematic wave approximation.

Once the bankful depth is exceeded in a given channel cell water may be routed into adjacent floodplain areas of the DEM. For each floodplain cell we merely know its dimensions, elevation and a user-defined friction coefficient. The simplest way to achieve distributed routing of water over the floodplain is to treat each cell as a storage volume for which we solve a continuity equation. The change in cell volume over time is therefore equal to the fluxes into and out of it during the time step

$$\frac{dV}{dt} = Q_{up} + Q_{down} + Q_{left} + Q_{right} \quad (3)$$

Where V is the cell volume [L^3], t is the time [T] and Q_{up} , Q_{down} , Q_{left} and Q_{right} are the flowrates (either positive or negative) from the upstream, downstream, left and right adjacent cells, respectively [L^3T^{-1}].

The flowrates between each cell can then be calculated using some uniform flow formulae. In this case we use the Manning equation, although it should be noted that a number of alternative uniform flow formulae could also be used such as the Chezy equation or the formulae for flow over free or drowned weirs. Thus the flowrate between two adjacent cells i and j , where i is the upstream cell, is equal to:

$$Q_{ij} = \frac{A_{ij} R_{ij}^{2/3} S_{ij}^{1/2}}{n} \quad (4)$$

where Q_{ij} is the flux [L^3T^{-1}] between cells i and j , A_{ij} is the cross sectional area [L^2] at the interface of the two cells, R_{ij} is the hydraulic radius [L] at the interface of the two cells, S_{ij} is the water surface slope between the two cells and n is the Manning friction coefficient [$L^{1/3}T^{-1}$], distinguishing between n_c for channels and n_{fp} for floodplains.

Table 1

Comparison of previous storage cell approaches with modelling flood inundation and standard hydraulic models with the new approach presented in this paper. Model complexity increases down table

Type/name of model	Authors	Channel routing	Floodplain routing	Discretisation	Application/validation
Planar water surface	Priestnall et al. (2000)	None	None	Planar surface is overlain onto either raster or TIN based Digital elevation models. All areas below the planar surface are considered flooded.	Applied to DEMs generated by the UK Environment agencies LiDAR data collection programme. No validation data were presented.
Storage cell	Cunge et al. (1976) and Romanowicz et al. (1996)	Uniform flow formulae (Manning and weir-type equations) using designated channel cells	Uniform flow formulae (Manning and weir-type equations)	Valley is split into channel and single cells representing the left and right floodplains.	Applied by Romanowicz et al. to an 11 km reach of the river Culm, UK using 285 cells. Validated against output from 2D FE scheme rather than field data.
Storage cell	Estrela (1994)	Uniform flow formulae (Manning and weir-type equations) using designated channel cells	Uniform flow formulae (Manning and weir-type equations)	Polygonal cells used for the floodplain, interlinked by channels. Cells follow existing natural boundaries and hence requires the user to discretise the floodplain. Several cells can be used in each floodplain cross section.	Applied to 250 km ² of the River Júcar floodplain, Spain using 403 cells. A 50 year recurrence interval flood was simulated and calibrated against an unspecified number of water depth observations. No validation data were presented.
Storage cell (FLOODSIM)	Bechteler et al. (1994)	One-dimensional model (no details given) running between floodplain cells	Uniform flow formulae (weir-type equations)	Triangular Irregular Network (TIN) with channels placed on the cell faces.	Applied to a 4 × 2.5 km reach of the River Rhine near Iffezheim and a 2 × 0.6 km reach of a river valley near Coburg. Simulations used up to 33 000 cells with a minimum resolution of 5 m. No validation data were presented.

Table 1 (continued)

Type/name of model	Authors	Channel routing	Floodplain routing	Discretisation	Application/validation
Storage cell (LISFLOOD-FP)	Bates and De Roo (this paper)	One-dimensional kinematic wave solved using an explicit finite difference procedure using designated channel cells	Uniform flow formulae (Manning equation)	Raster-based discretisation derived automatically from a DEM.	Applied to a major flood on a 35 km reach of the River Meuse using various resolution DEMs and up to 108 000 cells. Validated against high-resolution air photo and satellite-derived inundation extent data and gauging station records (see Section 3).
1D models (MIKE11, ISIS, ONDA, HEC-RAS, FLUCOMP among others)	Fread (1984) and Ervine and MacCleod (1999)	Full solution of the 1D St. Venant equations	Full solution of the 1D St. Venant equations	Treats domain as a series of cross sections perpendicular to the flow direction. Areas between cross sections are not explicitly represented	Typical application described by Penning-Rowse and Tunstall (1996). Here the ONDA code was applied to circa 20 km of the lower River Thames, UK using 1000 cross sections to define the channel/floodplain geometry. Validation has typically been undertaken against gauged records and, more infrequently, inundation extent.
2D Models (RMA-2, TELEMAC-2D, MIKE21, among others)	Feldhaus et al. (1992) and Bates et al. (1992) and Bates et al. (1995)	Full solution of the 2D St. Venant equations with turbulence closure	Full solution of the 2D St. Venant equations with turbulence closure	Structured grids (finite difference methods) or unstructured grids (finite volume and finite element methods) using a variety of geometries, but typically triangles or quadrilaterals.	Typical applications presented by Bates et al. (1998) for five river reaches between 0.5 and 60 km in length and using up to 15 000 triangular finite elements. Validated against dynamic water levels internal to the model domain and low resolution satellite imagery of flood inundation extent (Bates et al., 1997).

Table 2
Summary of model data and parameter requirements

Data requirement	Source	Comments
Raster Digital Elevation Model	Typically derived from air photogrammetry or airborne laser altimetry (LiDAR)	Grid resolutions of approximately 25–100 m would seem appropriate for most floodplain applications, although smaller resolutions are obviously preferable. Vertical accuracy of the DEM should generally be less than ~ 0.25 m.
Inflow discharge hydrograph	Gauging station records. Flow enters the model through the upstream channel cell forming the first location on the local drainage direction map.	Model can be used in either steady state or dynamic modes, but flows should be accurate to $\sim 10\%$. For dynamic simulations, temporal resolution depends on the speed of the hydrograph rise but typically at least hourly data are required.
Channel slope	Taken from the DEM or surveyed cross sections.	Can be set individually for each grid cell if necessary.
Channel width	Taken from the DEM or surveyed cross sections.	Can be set individually for each grid cell if necessary. Need not be the same as the model grid resolution.
Bankful depth	Taken from the DEM or surveyed cross sections.	Can be set individually for each grid cell if necessary.
Initial estimate of channel flow depth	Reasonable value based on experience and examination of surveyed cross sections and rating curves.	Model is run with constant in-bank discharge for a start up period to allow realistic channel water depths and flow velocities to develop. Start up period should be based on the time taken for flood waves to cross the domain.
Channel and floodplain friction	User defined parameters typically chosen with reference to published tables such as those given by Chow (1959) or Acrement and Schneider (1984)	N_c typically between 0.01 and 0.04. N_{ip} typically between 0.03 and 0.15. Can be set individually for each grid cell if necessary.
Model time step	User defined based on Courant number stability constraints. An explicit numerical scheme is used so the stability is a function of the cell dimensions and the flowrate. As water enters the model via a single inflow cell at the head of the reach, flowrates in this cell are usually the limiting factor.	Varies between applications but typical values are in the range 2–20 s.

Floodplain flow is thus approximated as a two-dimensional diffusion wave. As we use an explicit method, weights are introduced during the drying phase to prevent more water leaving a cell than it contains. To achieve this the flowrates Q_{up} , Q_{down} , Q_{left} and Q_{right} are calculated as above and then scaled by a non-dimensional coefficient c :

$$c = \frac{V_t}{(Q_{up} + Q_{down} + Q_{left} + Q_{right})\Delta t} \quad (5)$$

where V_t is the volume of water [L^3] in the cell at time t and Δt is the time step [T]. The water depth thus returns smoothly to zero as the cell dries out. Water can flow in any direction across the floodplain accord-

ing to the water surface gradient and local topography. This is important as floodplain depressions may fill from downstream if the topography permits. As the flood wave drains from the reach, water levels in the channel drop and the retreat of the inundation front is simulated. At the downstream boundary of the model water can leave the computational domain as either channel or floodplain flow. These are then summed to calculate the mass conservation error per time step:

$$E_t = \frac{(V_{in} - V_{out}) - (V_t - V_{t+1})}{V_{t+1}} \times 100 \quad (6)$$

where E_t is the mass balance error during time step t as a percentage of the volume of water in the domain at

the end of the time step [–], V_{in} and V_{out} are the volumes of water entering and leaving the domain during the time step [L^3], V_t is the total volume of water in the domain at the start of time step t [L^3] and V_{t+1} is the total volume of water in the domain at the end of the time step [L^3].

Boundary conditions for the model consist of an upstream inflow hydrograph that is assumed to enter at the inlet channel cell. No boundary conditions are applied at the downstream end of the model and water is able to leave freely with the flowrate calculation based on the local water slope between the penultimate and final cells. Initial conditions consist of an estimate of channel water depths along the reach at $t = 0$. Thus the floodplains are initially dry and the channel flow velocity is assumed to be zero. For large out-of-bank flows it might also be beneficial to assume that water enters the model via both the upstream channel and floodplain cells; however, this option has not been tested in the current paper.

The model was written in the PCRaster dynamic modelling language (Van Deursen and Wesseling, 1996; Wesseling et al., 1996), a GIS software designed to facilitate the rapid development of spatio-temporal models. This is a high level language that takes a raster map as its basic unit and whose commands consist of map operators combined with standard computational functions. In terms of computational efficiency the model performs approximately 100 floating point operations per grid cell per time step. This compares with approximately 4000 floating point operations per computational node per time step in a typical two-dimensional finite element code.

This approach is not new in concept and a similar method was first proposed by Cunge et al. (1976). Subsequently, similar methods have been used by Estrela (1994); Bechteler et al. (1994); Romanowicz et al. (1996). Although essentially similar, there are a number of differences between these approaches that are summarised, along with other flood inundation prediction methods, in Table 1. Table 1 demonstrates that the model proposed in this paper differs from the schemes proposed by Cunge et al. (1976), Estrela (1994) and Romanowicz et al. (1996) by including a one-dimensional dynamic routing model for channel flow rather than using uniform flow formulae and by the approach taken to discretising the floodplain. Typical applications of LISFLOOD-FP also include

approximately two orders of magnitude more computational cells. In principle, LISFLOOD-FP is similar to the FLOODSIM model of Bechteler et al. (1994) but has the advantage that model set up for a given DEM can be achieved automatically rather than requiring user intervention. Table 1 also demonstrates that storage cell models have not, to date, been validated against gauging station records and field observations of flood inundation extent. This is a significant omission and one that we here address for the first time in Section 3.

Data requirements for the model are summarised in Table 2. Thus the only user defined parameters are the values for channel and floodplain friction, n_c and n_{fp} . Whilst the parametrisation of the model is thus relatively parsimonious it should be recognised that considerable uncertainty generally surrounds the selection of appropriate friction coefficients for hydraulic models. The spatial and temporal variability of these parameters is usually unknown and hydraulic models are typically quite sensitive to the values chosen.

To apply the model, the DEM is first pre-processed to yield the local drainage direction map described above. Analysis of the DEM or surveyed cross section yields the channel geometry and the user defines appropriate friction coefficients and the model time step. The output from the model is a raster map of flow depth or free surface elevations at each time step and a discharge hydrograph at the downstream boundary. This can then be imported into standard GIS packages such as ARC-INFO.

3. Model testing

The model has been applied to a 35 km section of the River Meuse between the gauging stations at Borgharen (near the town of Maastricht) in The Netherlands and Maaseik in Belgium for which hourly discharge and stage records were available. This reach consists of a meandering channel approximately 100 m wide flowing across an extensive floodplain up to 3 km in width. In January 1995 severe flooding resulted in extensive inundation of the river valley, which was captured in both air photo imagery and by an overpass (see Fig. 1) of the ERS-1 Synthetic Aperture Radar (SAR) satellite system (De Roo et al.,

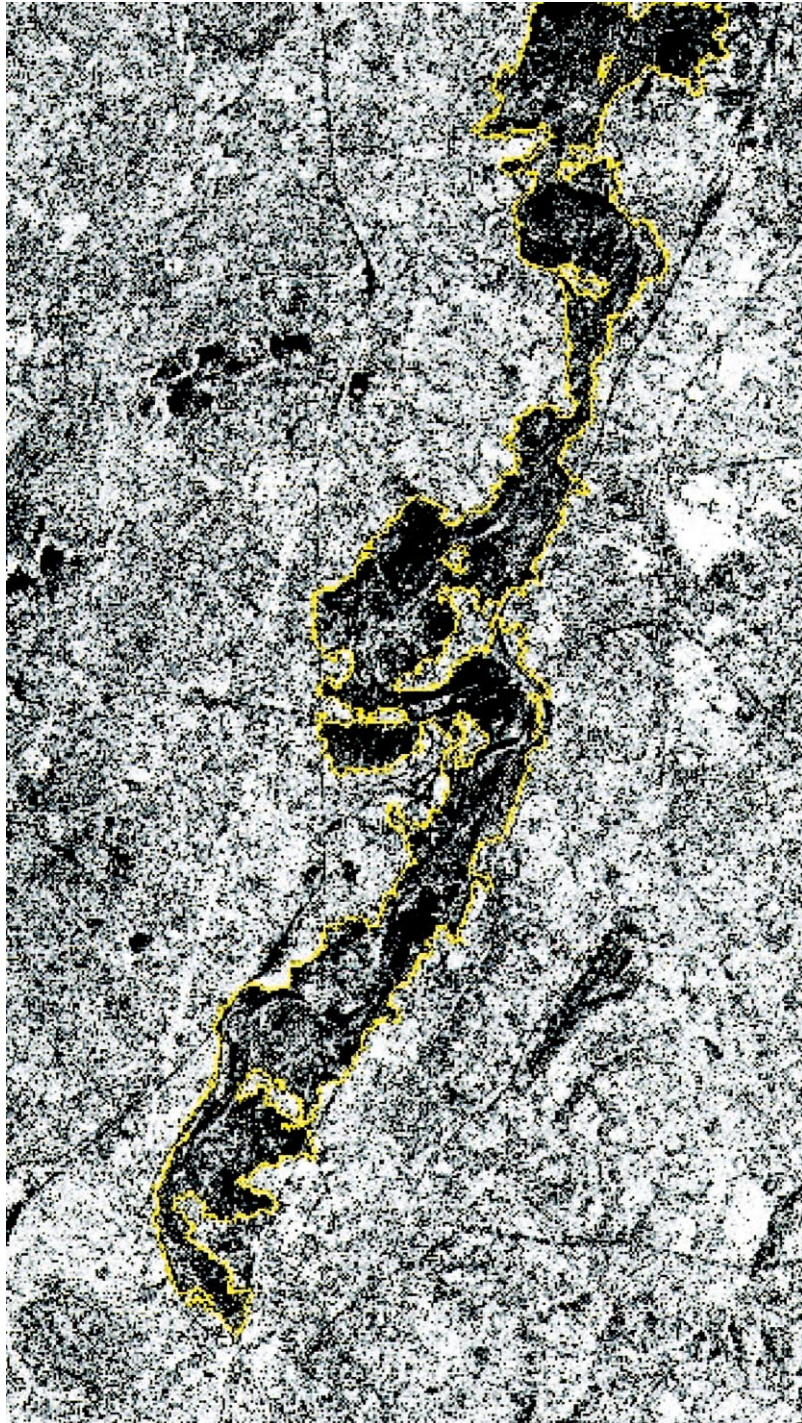


Fig. 1. ERS-1 SAR flooding on the River Meuse taken on the 30th of January 1995 at 1033 h. The results of the statistical snake inundation extent analysis are shown in yellow.

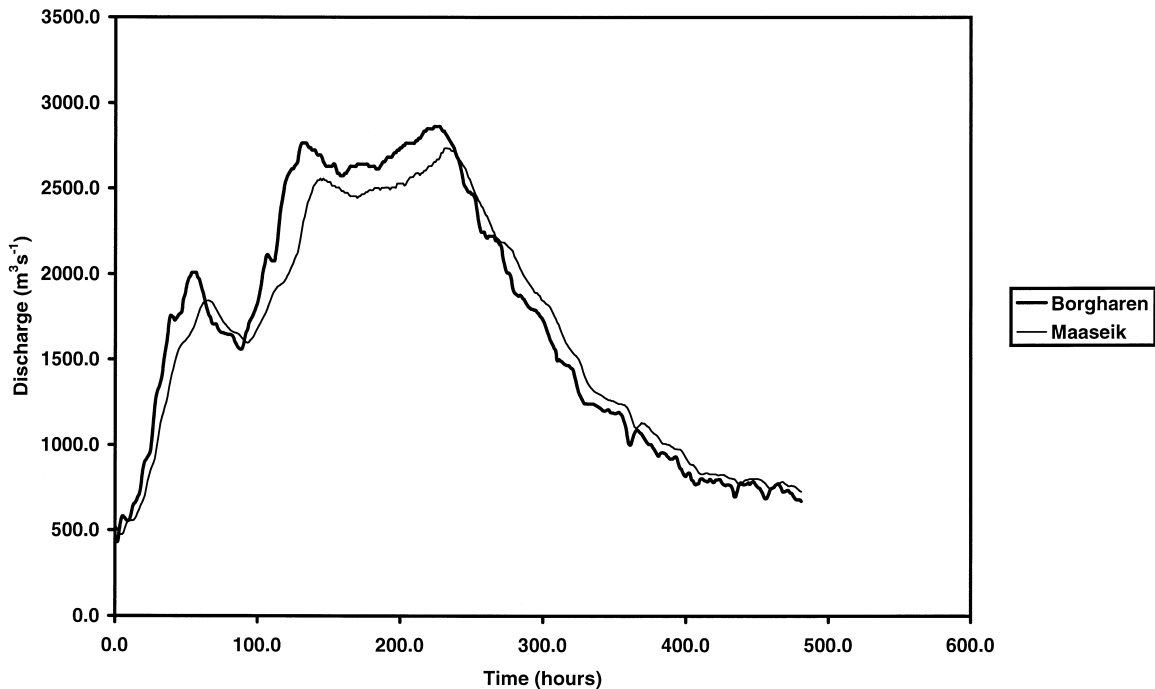


Fig. 2. Discharge hydrographs observed at the Borgharen and Maaseik gauging stations between 21st January 1995 and 11th February 1995. Peak flow occurred on the 31st of January with a discharge of $2863 \text{ m}^3 \text{ s}^{-1}$. The hydrograph peak took 8 h to travel between the two gauges and relatively little attenuation occurred.

1999b). In addition, a high resolution DEM of the reach has been assembled by the Dutch Water Authority (RWS) using airborne stereo-photogrammetry and ground survey conducted in 1995. This DEM consists of 329 354 points held within a TIN structure with an approximate horizontal resolution of 5 m and a quoted error of ± 5 cm in the horizontal and ± 6 cm in the vertical. Surveyed cross sections every 100 m are also available for this reach.

To apply the model the TIN-based Digital Elevation Model was converted into raster coverages at 25, 50 and 100 m resolutions using the ARC-INFO GIS software. This process provided a reasonable representation of the floodplain and did not result in either pits in the DEM or holes in levee structures for the 25 m DEM. Local drainage direction maps were then automatically extracted for each new DEM using the developed pre-processing sequence. Cross sectional geometry was taken from analysis of the surveyed channel cross sections, and, for simplicity, uniform values of width, slope and bankfull depth were chosen for the entire domain. Steady state flows were simu-

lated using the peak discharge ($2863 \text{ m}^3 \text{ s}^{-1}$) from the January 1995 event as measured at the upstream gauging station at Borgharen, whilst the discharge hydrograph from this site was used to drive dynamic simulations (see Fig. 2). Dynamic simulations commenced at 0000 hours on the 22nd of January, 1995 and continued until 0000 hours on the 11th of February. This represents 20 days or 480 h of real flow data. Peak flow occurred at the Borgharen gauge at 0700 hours on the 31st of January and at Maaseik at 1500 hours on the same day when a flow of $2736 \text{ m}^3 \text{ s}^{-1}$ was recorded. The hydrograph has a relatively broad and flat peak with flow above $2500 \text{ m}^3 \text{ s}^{-1}$ continuously recorded at Borgharen between the 26th of January and the 1st of February. The wave travel time was relatively fast (8 h) and little attenuation occurred through the reach. The SAR overpass occurred on the 30th of January at 1033 hours when the discharge at Borgharen was $2516 \text{ m}^3 \text{ s}^{-1}$. The air photo survey was conducted on the 27th of January when the maximum discharge at Borgharen was $2558 \text{ m}^3 \text{ s}^{-1}$ and water levels along

Table 3

Data sources and parameters used in the application of LISFLOOD-FP to the river Meuse

Data requirement	Source	Value
Raster Digital Elevation Model	Air stereo-photogrammetry	25, 50 and 100 m resolutions derived from a 5 m resolution TIN with vertical accuracy of ± 6 cm
Inflow discharge hydrograph	Gauged hydrograph at Borgharen (The Netherlands)	20 day flood event with peak discharge of $2863 \text{ m}^3 \text{ s}^{-1}$.
Channel slope	Surveyed cross sections	0.0004 m m^{-1}
Channel width	Surveyed cross section	100 m
Bankful depth	Surveyed cross section	3 m
Initial channel flow depth	Rating curves from the Borgharen and Maaseik gauges	1 m
Channel and floodplain friction	Typical values from Chow (1959) and Acrement and Schneider (1984)	$N_c: 0.02$. $N_{fp}: 0.06$.
Model time step	User defined as a function of flowrate and cell dimensions	25 m DEM: 2 s. 50 m DEM: 5 s. 100 m DEM: 10 s.

the reach measured by the Dutch Water Authority (RWS) were approximately 10 cm lower than those recorded at peak flow. Thus, despite the different sampling periods for the observed data, variations between data sets due to different hydraulic conditions should be relatively small. The return period of the event has been estimated as 1 in 63 years. Model data sources and parameters are summarised in Table 3. Importantly, calibration of friction factor values was not undertaken and we have merely selected typical values suggested in the available literature (Chow, 1959; Acrement and Schneider, 1984). However, as with all hydraulic models sensitivity to friction factor values is to be expected in dynamic simulations and examination of model response to friction parameter variation should be a part of any further study.

A summary of the simulations performed is given in Table 4. Steady state simulations were undertaken for the full reach at 25, 50 and 100 m resolutions and

dynamic simulations at 50 and 100 m. However, to reduce computational requirements a 7 km section of the 25 m resolution DEM below the gauging station at Borgharen was extracted. This was then used to undertake the 25 m resolution dynamic simulation. A steady state simulation was also performed on this smaller DEM. The initial water depth in the channel was assumed to be 1 m for all simulations, a value consistent with the discharge of $429 \text{ m}^3 \text{ s}^{-1}$ recorded at Borgharen at 0000 hours on the 26th January (the start of the dynamic simulation). To allow realistic channel water depths and velocities to develop prior to dynamic simulations, a constant inflow at this discharge was simulated for 8 h prior to the real hydrograph data. This period was chosen on the basis of the observed wave travel time between the Borgharen and Maaseik gauges. Steady state simulations used a discharge hydrograph that increased linearly from 429 to $2863 \text{ m}^3 \text{ s}^{-1}$ (the peak discharge

Table 4

Summary of simulations performed

Simulation	Reach length (km)	Number of grid cells	Number of time steps	Validated against
25 m DEM, steady state	7	20 650	100 000	Air photo and SAR derived inundation
25 m DEM, dynamic	7	20 650	864 005	Air photo and SAR derived inundation
25 m DEM, steady state	35	108 464	120 000	Air photo and SAR derived inundation
50 m DEM, steady state	35	27 110	50 000	Air photo and SAR derived inundation
50 m DEM, dynamic	35	27 110	345 602	Air photo and SAR derived inundation
100 m DEM, steady state	35	6958	25 000	Air photo and SAR derived inundation
100 m DEM, dynamic	35	6958	172 801	Air photo and SAR derived inundation. Gauged discharge and stage at Maaseik (downstream)

recorded at Borgharen) over an 8 h period and then remained constant at this level. Simulations were then allowed to run until the water depths predicted by the model ceased to show any variation. Simulations were undertaken on a Pentium II PC running at 450 MHz. Memory usage is a function of the number of grid cells and was therefore at a maximum for simulations with the 25 m full reach DEM, which took up approximately 110 Mb of RAM.

Simulations were validated against the shorelines observed from air photography and SAR imagery and, in the case of dynamic simulations on the full reach model, against observed discharge and stage at the downstream gauging station (Maaseik). Unlike most higher order hydraulic codes, which require both upstream and downstream boundary conditions (see for example Bates et al., 1998), the LISFLOOD-FP model only requires an upstream inflow hydrograph. Additional gauging stations both internal to the domain and at the downstream outlet are thus fully independent of the model and may be used as validation data. The air photo imagery was converted into a shoreline by the Dutch Water Authorities (RWS) and has an approximate horizontal accuracy of 25 m. The SAR imagery was processed in two different ways: using a standard thresholding technique (see for example Tholey, 1995; Imhoff, 1997) with a horizontal resolution of 25 m and a newly developed statistical active contour model or ‘snake’ (Horritt, 1999). The central problem with all SAR image processing is how to combat the high level of noise (or speckle) evident in Fig. 1, without the degradation in spatial resolution associated with many local averaging techniques (for a full review see Horritt, 1999). The snake algorithm deals with this by measuring local speckle statistics along the shoreline and is thus able to segment the shoreline to an accuracy of ~ 1 pixel (12.5 m for ERS-1 SAR). However, problems may still occur as increased back scattering of the radar signal by wind roughening of the water surface and particular land use types can lead to misclassification of flooded areas, hence the use of more than one processing method. In general, misclassification errors will be greater with the SAR data than the low altitude airborne survey, and the latter is likely to be the data set closest to the true shoreline.

Model ability was assessed by comparing the inundated area derived from the air photo and SAR data,

IA_{obs} , with the inundated area predicted by the model, IA_{mod} . Deriving appropriate areal statistics is not straightforward, however one possible measure of fit is given by:

$$\text{Fit}(\%) = \frac{IA_{\text{obs}} \cap IA_{\text{mod}}}{IA_{\text{obs}} \cup IA_{\text{mod}}} \times 100 \quad (7)$$

This measure is equal to 100% when the two areas coincide, and penalises over- and underprediction of inundated areas by the model. An alternative measure is to calculate the number of pixels classified correctly as either wet or dry as a percentage of the total area. To perform these calculations the inundation boundary vectors derived from analysis of the air photo and SAR data were first converted into 25 m raster coverages, using a binary wet/dry classification for each pixel. Model results from the 50 and 100 m resolution simulations were then re-sampled on to a 25 m grid and again classified as being either wet or dry. With observed and model data classified at an identical resolution, fit and percentage correct statistics could be calculated. These, along with mass balance errors for each simulation, are given in Table 5, with statistics for the dynamic simulations calculated at the time of the SAR overpass.

Model performance was compared to inundated area predictions obtained using two other methods: a planar approximation to the free surface based on a linear interpolation of maximum water surface elevations recorded at the Borgharen and Maaseik gauges and a preliminary steady state simulation with a two-dimensional finite element model. The finite element mesh and topography is shown in Fig. 3 and consists of 9639 nodes and 18 939 elements. This is at the current feasible limit for dynamic simulations of the duration of the Meuse event on a relatively high powered workstation and allows element sizes in the range 50–250 m, where the smaller elements are closer to the channel. The finite element model is thus relatively coarse compared to the grids used in the raster model, but has a higher level of process representation. The steady state finite element simulation was undertaken using the peak discharge at Borgharen and the peak water surface elevation at Maaseik as upstream and boundary conditions, respectively and identical friction parameters to those used in the raster model. The model solves the Shallow Water equations at each computational node

Table 5

Summary of results for the seven model simulations. As a comparison, the results obtained using a planar approximation to the free surface and a two-dimensional finite element model are also shown

Simulation	Mass balance error per time step as a percentage of volume in the domain	Total mass error over the simulation as a percentage of inflow hydrograph volume	Fit and % correct for air photo derived inundation		Fit and % correct for snake algorithm derived inundation		Fit and % correct for threshold algorithm derived inundation	
			Fit (%)	Correct (%)	Fit (%)	Correct (%)	Fit (%)	Correct (%)
25 m 7 km DEM, planar surface	–	–	80.4	83.7	67.0	71.2	76.1	78.7
25 m 7 km DEM, steady state	0.001	0.77	81.6	85.5	70.9	76.4	77.1	80.6
25 m 7 km DEM, dynamic	0.001	1.82	80.6	84.9	71.1	76.9	75.7	79.5
25 m 35 km DEM, planar surface	–	–	64.0	69.5	53.3	58.0	61.2	64.4
25 m 35 km DEM, steady state	0.0002	5.4	77.3	81.9	77.2	81.1	74.3	77.6
50 m 35 km DEM, planar surface	–	–	63.8	69.4	53.4	58.1	61.1	64.3
50 m 35 km DEM, steady state	0.0008	4.86	78.3	81.6	68.5	72.1	75.7	77.9
50 m 35 km DEM, dynamic	0.0009	8.45	77.1	80.6	69.1	72.4	75.5	77.5
100 m 35 km DEM, planar surface	–	–	63.3	69.2	53.1	57.8	60.9	64.1
100 m 35 km DEM, steady state	0.0004	3.51	69.2	70.2	66.0	66.4	75.6	75.9
100 m 35 km DEM, dynamic	0.0005	5.04	69.6	70.9	65.7	66.2	75.1	75.4
2D FE model (element sizes in the range 50–250 m)	1×10^{-5}	0.04	48.1	56.2	49.9	56.8	58.2	63.8

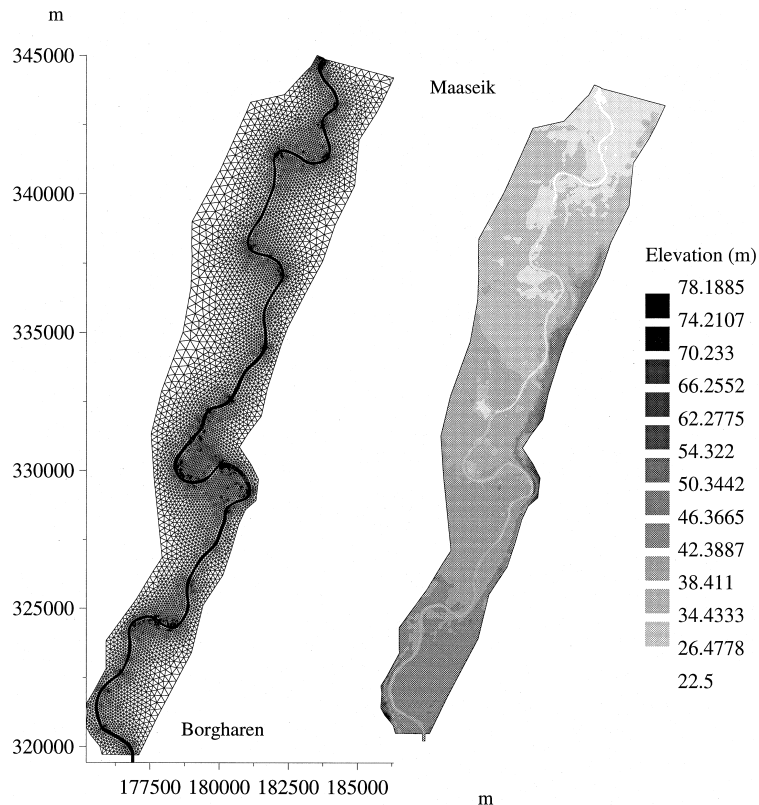


Fig. 3. Finite element mesh and topography developed for the River Meuse between Borgharen and Maaseik. The mesh consists of 9639 nodes and 18 939 elements.

using an implicit finite element scheme and, for simplicity, a zero equation turbulence closure model with the turbulent eddy viscosity set to $0.1 \text{ m}^2 \text{ s}^{-1}$.

4. Discussion

In general, the air photo shoreline is best predicted by the raster model, closely followed by the threshold algorithm shoreline. The comparison between the model and the snake algorithm shoreline is typically 5–10% lower for both model performance measures and would seem to be due to the way this algorithm treats urban areas on the floodplain in the vicinity of Borgharen. These are classified as flooded by the air photo and the threshold algorithm but as dry by the snake method. The model uniformly predicts these areas as flooded and this accounts for much of the variation. This is shown in Fig. 4, which provides a

comparison of model predicted water depths for the steady state 25 m DEM model with the shorelines derived from the air photo data and the two SAR processing methods for the area below the gauging station at Borgharen. The urban areas are located on the right bank and are denoted as (a) and (b) on the figure. For the most part the three observed shorelines are rather similar apart from in the vicinity of these urban areas. The model shows a reasonable fit to the observed shorelines for most of the reach, and even manages to replicate two islands in the middle of the floodplain observed in the air photo data on the southern (downstream) right bank. Considerable structure can also be seen in the predicted depths as the DEM is able to resolve levees, old channels and floodplain depressions. However, the model does underpredict inundation for a portion of the right bank. Similar analysis for the 50 and 100 m DEM steady state simulations and the planar surface approximation applied

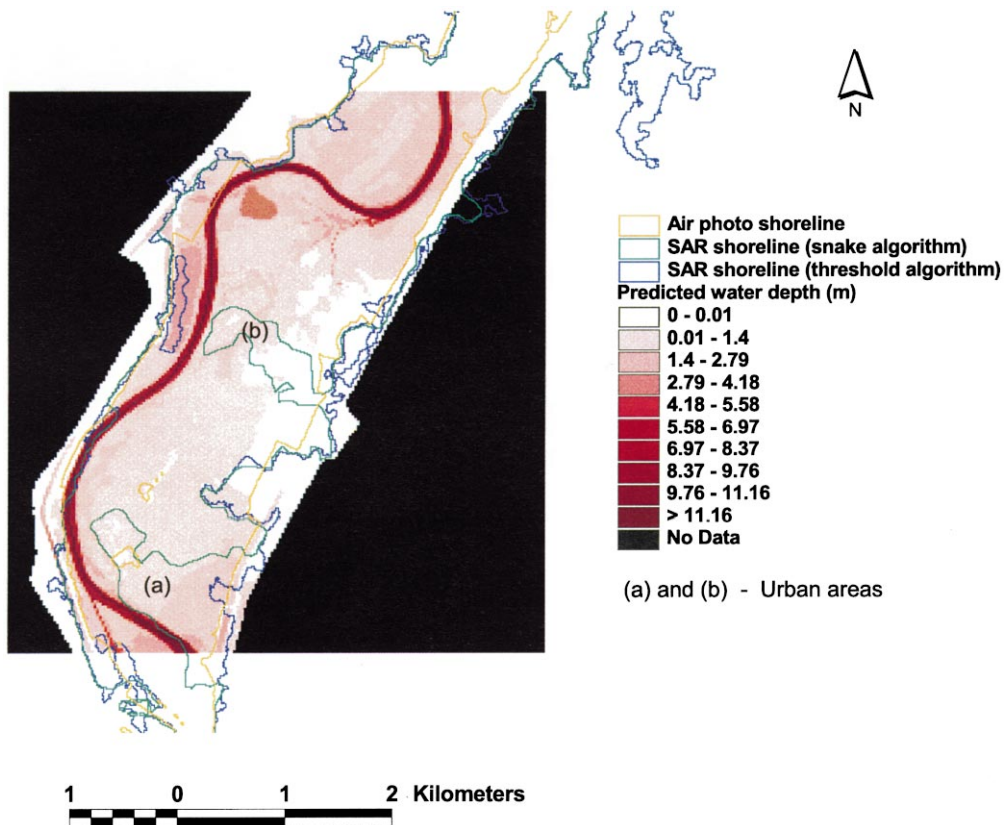


Fig. 4. Comparison of water depths predicted by the 25 m resolution steady state raster model to air photo and SAR-derived shorelines for a portion of the model domain downstream of the Borgharen gauging station.

to the 50 and 100 m DEMs showed progressive deterioration in predictive ability. Whilst the floodplain flow depths for the 50 m simulation were physically reasonable those predicted by the 100 m model were rather high (greater than 4 m). This was probably due to the smoothing out of levee structures in the 100 m DEM, which allowed more water onto the floodplain.

Table 5 demonstrates that at the reach scale the raster inundation model provides a significant improvement in inundation prediction ability over either of the two alternative methods considered. Concentrating on the comparison with air photo data, as this is assumed to be closest to the 'true' shoreline, the best fit raster model (25 m DEM, steady state simulation 35 km reach) correctly predicts 81.9% of pixels as wet or dry compared with only 69.5% for the best fit planar approximation (also on the 25 m DEM for the 35 km reach). The planar

approximation is therefore rather poor, as if we assume that the floodplain (as defined by the DEM) is completely inundated we would correctly predict 67.2% of pixels classified from the air photo data. The fit statistic for this assumption would also be 67.2%. This then is the lower limit of predictive ability acceptable from a simulation model and the best reach scale planar approximation only improves on this by 2.3%.

At the reach scale there is only a 0.3% improvement in the predictive ability of the planar surface approximation as the DEM resolution increases. For the case of the 100 m DEM both the raster model and planar approximation perform equally well (respectively 70.2 and 69.2% of pixels are predicted correctly). However as the resolution increases the raster model prediction improves markedly. Nevertheless, in certain situations the planar approximation can

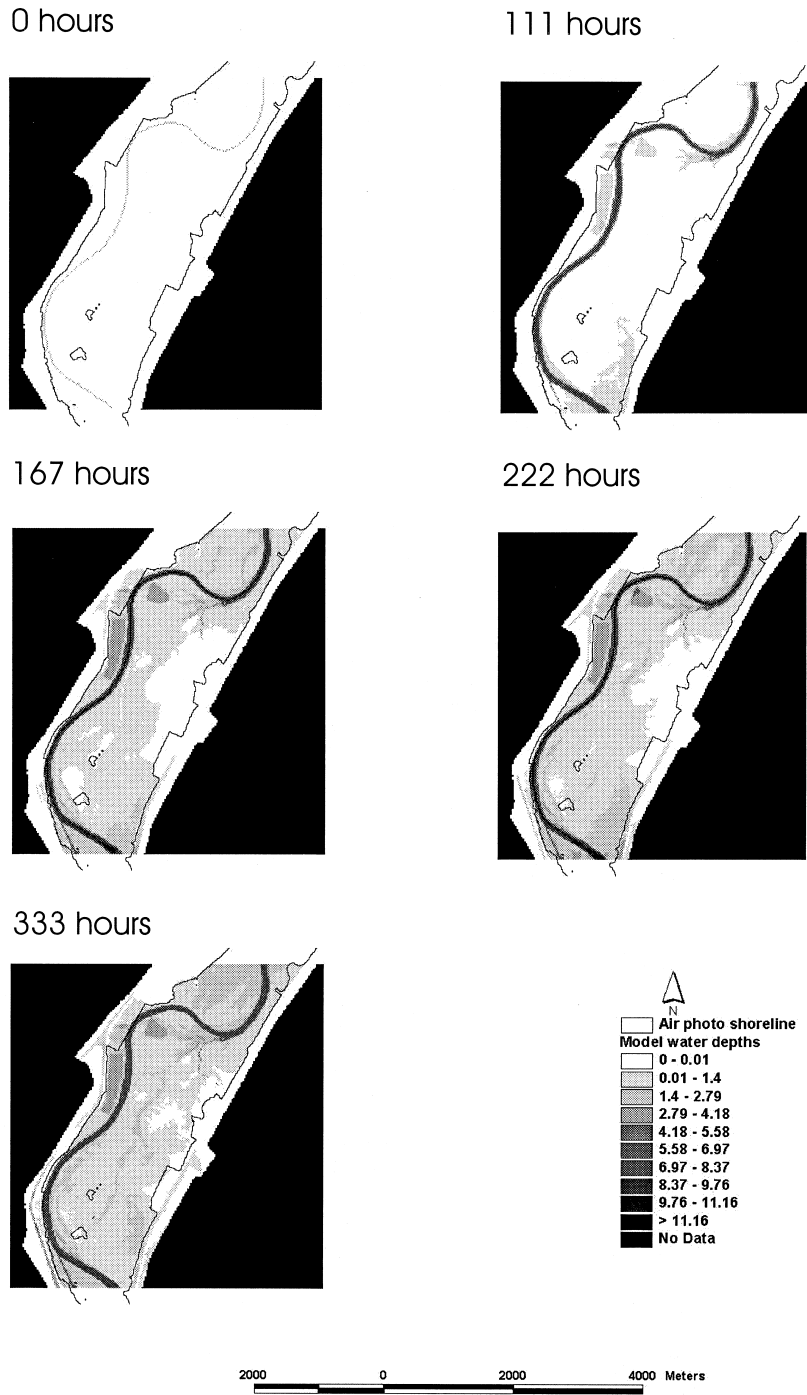


Fig. 5. Time series of inundation extent predicted by a dynamic simulation of the raster model using a 25 m resolution DEM for the 7 km reach downstream of the Borgharen gauging station. This is compared to the air photo derived shoreline sampled at approximately 160 h into the simulation.

provide inundation predictions that are almost as good as those that can be obtained from the raster model. For the 25 m DEM developed for the 7 km reach below Borgharen the planar approximation correctly predicts 83.7% of pixels compared with 85.5% for the steady state simulation performed with the raster model. This is probably due to the fact that one of the control points for the planar surface was the maximum water elevation for the Borgharen gauge. One would assume that the planar approximation would work less well further away from its control points and examination of the performance for the full reach planar approximation at 25 m resolution in Table 5 shows this to be the case. However, for short reaches of relatively straight channel and steep floodplain lateral slopes where good control data exists the planar approximation may perform adequately. The problem, however, is that no objective criteria currently exist to enable such situations to be identified, whereas the performance of the raster model seems solely to depend on having a Digital Elevation Model of sufficient resolution. The raster model is also capable of dynamic prediction as demonstrated in Fig. 5, which shows the development of inundation on the 7 km 25 m resolution DEM. This is compared with the air photo shoreline that was sampled approximately 160 h into the simulation. The model indicates that the inundation field continues to extend after this time and this is consistent with the known hydraulics of the event. In general, however, the dynamic simulations are marginally less good predictors of inundation extent than the steady state models. This may be due to the hydraulics of this particular event, where the broad flat hydrograph peak leads to relatively little transient behaviour. This also means that despite having two inundation extent data sets sampled four days apart, the validation process tells us relatively little about the dynamic ability of the model and further testing is required here. This can be problematic as inundation extent data only tend to be collected for the largest floods on major lowland rivers where there is sufficient lead time to organise deployment of sampling resources. Such events tend not to be highly dynamic and are thus not ideal for testing this aspect of model performance.

Mass balance errors for the raster model are acceptably low when considered in terms of a percentage

error per time step and, as might be expected, these errors increase with decreasing cell size and increasing number of cells. However, given the large number of time steps simulated and the large number of cells in certain models the cumulative error for particular simulations can become quite large (up to 8.45%). This should be addressed in future research and is probably a result of coding the model in single rather than double precision and the choice of a rather basic numerical scheme for the channel routing.

The finite element model provides a relatively poor representation of the inundated area (63.8% correct at best) due to the coarse nature of the finite element discretisation compared with the highest resolution raster grids. Water depths predicted by the finite element model are shown in Fig. 6 and seem to be rather more realistic than for the 100 m DEM model. This seems to suggest that if both models were configured at a similar resolution then the finite element model would outperform the raster-based code. It is also clear that inundation is strongly controlled by topography. It may be that the finite element model will always outperform the simpler code at a given resolution or, alternatively if the topographic control is overwhelmingly dominant, that at a certain resolution the results of the two models will converge. In the latter case the simpler model should always be favoured. At present it is impossible to determine which of these two hypothesis is correct; however, as dynamic finite element simulations at a resolution comparable to the 25 m raster grid are not currently computationally feasible for events of the length of the Meuse flood, the raster-based scheme would seem to be the only way to proceed for dynamic reach scale simulations. If, however, the raster model simulations are correct in identifying steady state simulations as sufficient to allow peak inundation extent prediction for at least certain classes of flood events, more resolved finite element schemes may be entirely feasible. There are also a number of refinements to the finite element model that could also be implemented including higher order turbulence closure schemes and more sophisticated algorithms to correct for dynamic wetting and drying (see for example Bates and Hervouet, 1999). Moreover, it should be noted that the finite element model does produce a variety of other outputs, such as flow velocities, which may also be required for particular applications.

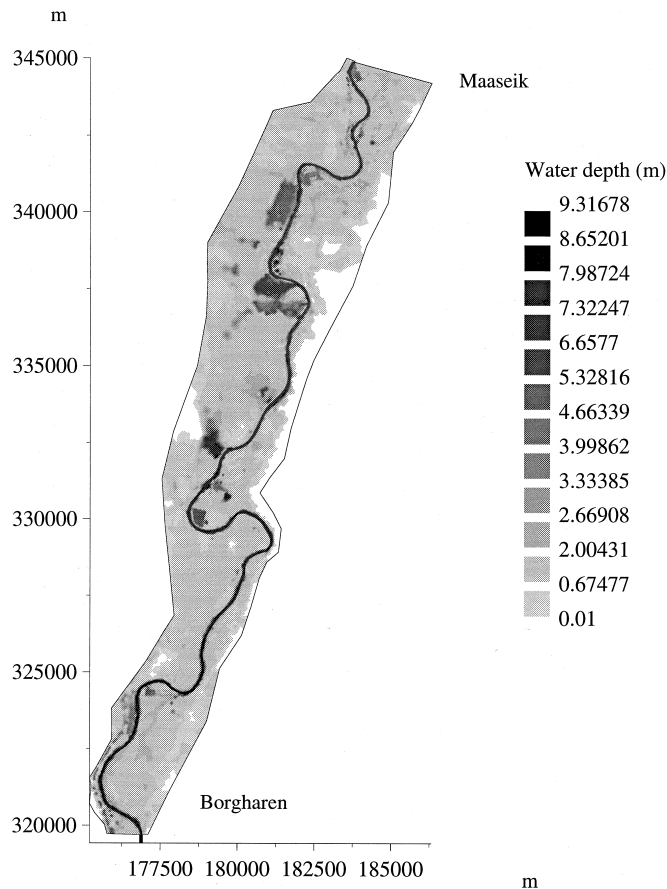


Fig. 6. Water depths predicted by the finite element model for the Borgharen to Maaseik reach. Despite the coarse grid size (50–250 m) the water depths would appear to be more physically realistic than those predicted by the 100 m resolution raster model. However, the absolute model performance is relatively poor compared with the best fit raster model simulations.

The 100 m resolution reach scale dynamic model was also validated against the stage and discharge hydrographs recorded at the Maaseik gauge (see Figs. 7 and 8). Given that the main aim of the model was to predict inundation extent, these results are quite encouraging. The routing performance of the model is relatively good given its simplicity, particularly for the discharge hydrograph, which is probably within the error of the observed data for such a large event. The 100 m resolution model overpredicts stage as would be expected from a consideration of the simulated floodplain water depths, yet still the maximum error is only about 80 cm.

Finally, error distributions from the raster model were analysed in terms of the distance of under- or

overpredicted pixels from the nearest shoreline observed in the air photo data. This distance, in terms of number of model pixels, was calculated for each incorrectly predicted grid cell in each resolution model and for dynamic, steady state and planar approximations to the free surface. The distance in terms of number of pixels was then converted into an absolute distance range to facilitate comparison between different resolution models. These are shown in Fig. 9a–c. Thus for the 100 m resolution models approximately 30% of pixels are incorrectly predicted as either dry when they should be wet or vice versa. Fig. 9a shows the number of incorrectly predicted pixels (as a percentage of all the pixels in the model) that are 100–200 m from the observed shoreline, 200–300 m, 300–400 m and so on. The

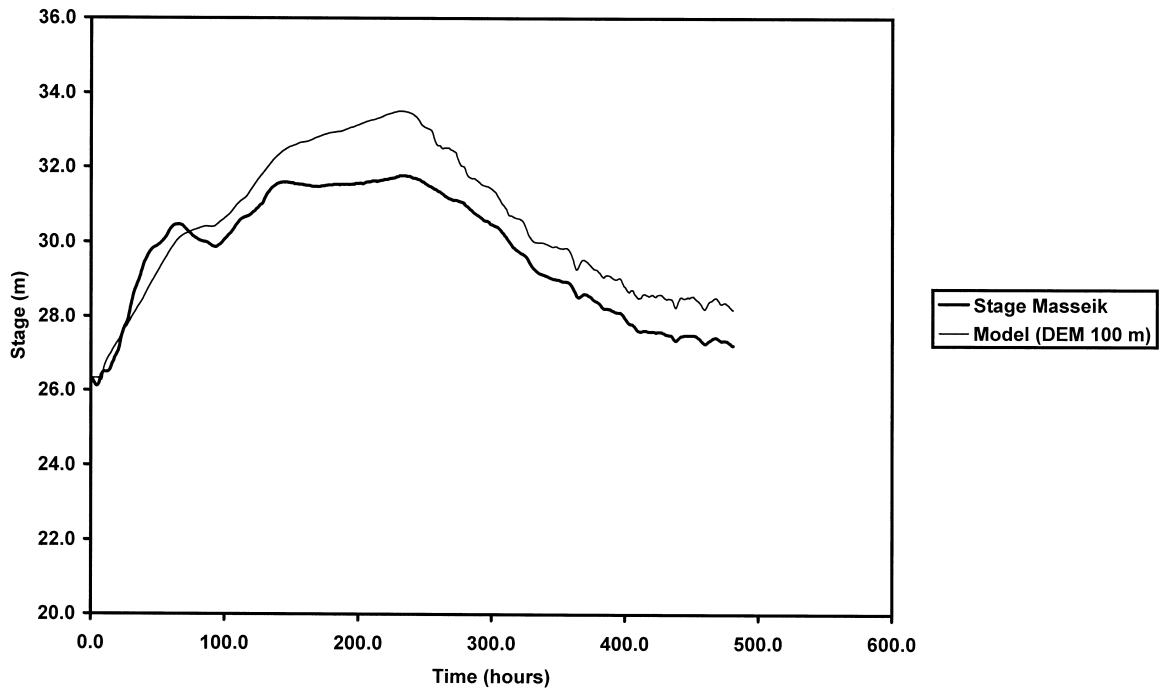


Fig. 7. Comparison of the water surface elevation hydrograph observed at the Maaseik gauging station with predictions from a dynamic simulation obtained with the 100 m resolution raster model.

resolution of the distance bands and their lower limit is thus controlled by the resolution of the model. The error distributions thus become progressively smoother as the model resolution decreases, although for simplicity some of the higher distance bands have been amalgamated for the 25 and 50 m resolution models. Fig. 9 shows that the majority of model errors tend to be relatively small and that in most cases the raster model outperforms the planar surface approximation. The 25 m resolution dynamic model applied to the 7 km reach below Borgharen does, however, show a distinct group of mis-predicted pixels some 600 m from the shoreline although the absolute number of pixels with this level of error is relatively low and within the error of the data source.

Given the errors in the observed data it is perhaps best not to over-interpret these error distributions or model results. Indeed, if one takes the air photo as 'ground truth' the overlap with the SAR-derived inundated area calculated using the threshold and snake techniques is only 83.3 and 81.0%, respectively. The best fit model could thus be considered to be at the

current prediction limit for this class of problem. This is particularly true if one takes account of the ± 25 m error in shoreline position that we have assumed is associated with the air photo data. Fig. 9c shows that 2.2% of the total number of model pixels in the best fit simulation (25 m DEM, steady state) are, if mis-classified, within ± 25 m of the 'true' shoreline. This is equivalent to a 1 pixel error in shoreline location at this model resolution. This figure rises to 3.8% within ± 50 m or 2 pixels. If these error bands are added to the percentage of pixels correctly predicted by the model the total model accuracy becomes 87.7% for a ± 25 m error and 89.3% for a ± 50 m error for the 7 km reach. Given the variations in the observed inundation data sets and typical gauging station errors for large out-of-bank flow events this would seem to be as accurate as it is currently possible to achieve. Whilst more complex codes might show an apparent improvement in predictive ability it would be difficult with current data sources to tell whether or not this was justified.

The central question of model identifiability

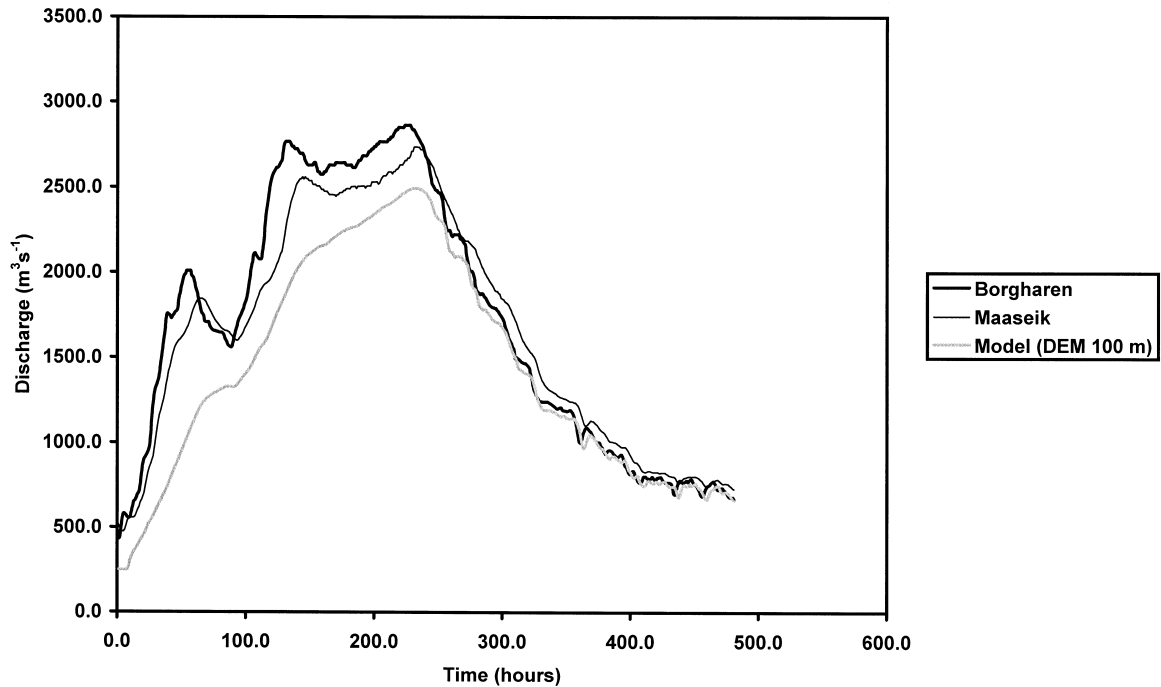


Fig. 8. Comparison of the discharge hydrograph observed at the Maaseik gauging station with predictions from a dynamic simulation obtained with the 100 m resolution raster model.

addressed by this paper is therefore unresolved. Whilst the planar approximation has been shown to yield acceptable results in particular circumstances, these cannot be anticipated a priori and it is thus difficult to assign a confidence level to such predictions. On the other hand the available data do allow identification of an optimum hydraulics-based approach. The raster model developed in this paper does have a number of advantages in terms of simplicity, low computational cost and ready integration with newly available high-resolution data sources. However, it may be that other storage cell models or more complex one- and two-dimensional hydraulic codes could perform equally well if applied at the same resolution, and the simulations reported do begin to define what this resolution might be. In effect the question of model choice for flood inundation prediction remains open, yet uncertainties over validation will almost invariably occur for environmental problems and in this situation the simplest explanation that fits the evidence should perhaps be favoured.

5. Conclusions

This paper has sought to develop an accurate scheme for predicting flood inundation extent. A variety of approaches have been tested and best results obtained with the raster-based code developed in this paper. Unlike other hydraulic models this scheme was specifically designed to predict flood inundation and ignored or minimised the representation of processes that were not considered central to this aim. The model was designed to work with high-resolution topographic data that are, or in the near future will be, widely available. In particular, it was specifically designed to rely fully on published sources and not require any additional data collection. Inundation prediction ability was maximised at the expense of other aspects of the hydraulics, such as flood routing, yet the model was still able to reproduce observed hydrograph data to a reasonable level. A key factor in the model development process was the search for the simplest solution that fitted the available data. This is different to a great deal of current modelling

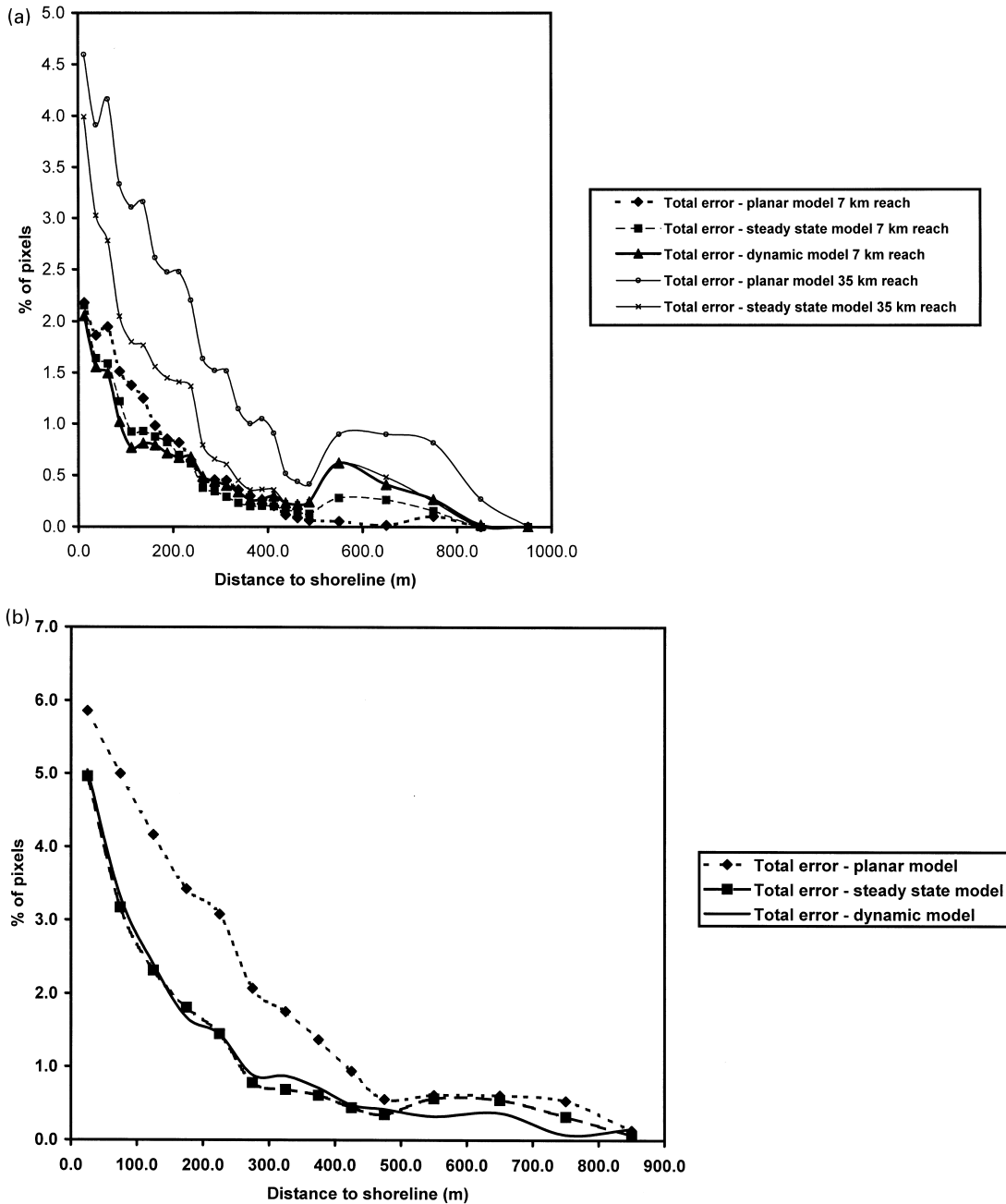


Fig. 9. Error distributions for under- and overpredicted pixels in the: (a) 100; (b) 50; and (c) 25 m, resolution raster model simulations. For each of the simulations the minimum distance from each under- or overpredicted pixel to the 'true' shoreline in the air photo data is calculated. The percentage of the total number of pixels falling within 1 pixel error bands are then calculated.

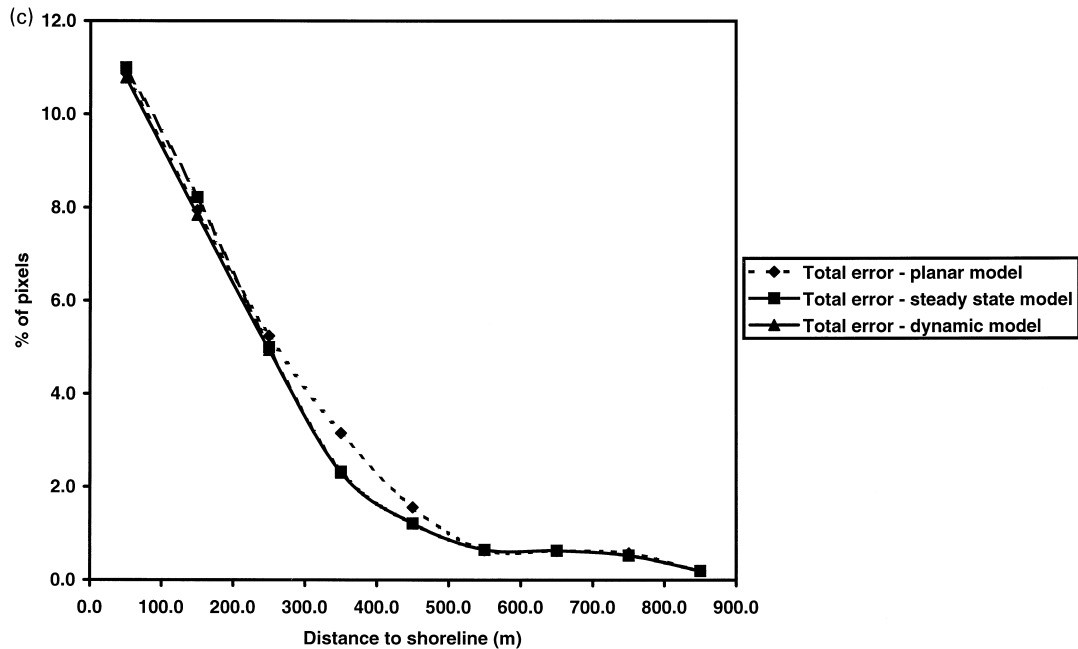


Fig. 9. (continued)

activity, yet should actually be our primary focus as modellers.

The analysis undertaken demonstrated that the model is currently at the limit of predictive ability for flood inundation problems. Given the differences between the air photo and satellite-derived data sets and a consideration of likely errors associated with each of these sources, a significant degree of uncertainty surrounds inundation extent observations. Using the raster analysis of the Meuse data we estimate that even the best inundation extent observations only capture 90% of the 'true' flooded area. Thus a model capable of matching a given inundation data set to this level of accuracy is within the error envelope of the validation data source and beyond this apparent improvements in model performance cannot be effectively tested. The only solution here is to collect better inundation extent and gauging station records or, if this cannot be achieved, to use the model within an uncertainty analysis framework (cf. Romanowicz et al., 1996).

Future work should examine more closely the impact of changing resolution on model performance and undertake more detailed comparison with predictions obtained with two-dimensional, and other,

hydraulic modelling techniques. In particular, we should perhaps look at the use of steady state two-dimensional models with a resolution an order of magnitude greater than that used in this paper, as it appears that for events like the January 1995 Meuse flood dynamic effects may be relatively unimportant in terms of peak inundation extent prediction. This is however a rather tentative conclusion and one that requires further confirmation. Indeed one of the limitations of the validation exercise conducted in the present study is that, despite the use of one of the best flood inundation data sets available, only partial testing of the dynamic predictions of the raster model could be undertaken. In general, substantially more validation is required. It may also be possible to boost computational performance in a number of ways including substituting an implicit numerical method for the explicit scheme used to solve the kinematic wave equation used for channel routing. This might also help in reducing the mass balance error, as would re-coding the model using double precision variables. Finally, there are a number of process enhancements that could be implemented including use of diffusion or full dynamic wave routing for the channel flow and implementing some algorithm to

simulate the momentum exchange that occurs across the shear layer between main channel and floodplain flows. However, whilst these would improve the model process representation they would seem to be unnecessary on the basis of currently available data.

Acknowledgements

Our thanks go to the RWS Maastricht for allowing access to the air photo inundation extent data, DEM, surveyed cross sections and flow discharge data. The Belgian Water Authorities also kindly allowed access to gauging station records from Maaseik. Matt Horritt of the University of Bristol provided results from the 'snake' SAR algorithm analysis and advised on model validation. Johan Van Der Knijff of JRC, Ispra performed the SAR threshold algorithm analysis. Funding for this research was also obtained from the UK Natural Environment Research Council grant number GR3 CO/030.

References

- Acement, G.J., Schneider, V.R., 1984. Guide for Selecting Manning's Roughness Coefficients for Natural Channels and flood plains. Federal Highways Administration, US Department of Transportation, Report No. FHWA-TS-84-204, Washington, 62 pp.
- Bates, P.D., Hervouet, J.-M., 1999. A new method for moving boundary hydrodynamic problems in shallow water. *Proceedings of the Royal Society of London, Series A* 455, 3107–3128.
- Bates, P.D., Anderson, M.G., Baird, L., Walling, D.E., Simm, D., 1992. Modelling floodplain flow with a two-dimensional finite element scheme. *Earth Surface Processes and Landforms* 17, 575–588.
- Bates, P.D., Anderson, M.G., Hervouet, J.-M., 1995. Initial comparison of two two-dimensional finite element codes for river flood simulation. *Proceedings of the Institution of Civil Engineers, Water Maritime and Energy* 112, 238–248.
- Bates, P.D., Horritt, M., Smith, C., Mason, D., 1997. Integrating remote sensing observations of flood hydrology and hydraulic modelling. *Hydrological Processes* 11, 1777–1795.
- Bates, P.D., Stewart, M.D., Siggers, G.B., Smith, C.N., Hervouet, J.-M., Sellin, R.H.J., 1998. Internal and external validation of a two-dimensional finite element model for river flood simulation. *Proceedings of the Institution of Civil Engineers, Water Maritime and Energy* 130, 127–141.
- Bechteler, W., Hartmaan, S., Otto, A.J., 1994. Coupling of 2D and 1D models and integration into Geographic Information Systems (GIS). In: White, W.R., Watts, J. (Eds.). *Proceedings of the 2nd International Conference on River Flood Hydraulics*, John Wiley and Sons, pp. 155–165.
- Chow, V.T., 1959. *Open channel hydraulics*, Mc-Graw Hill, New York.
- Chow, V.T., Maidment, D.R., Mays, L.W., 1988. *Applied hydrology*, Mc-Graw Hill, New York (572 pp.).
- Cunge, J.A., Holly Jr., F.M., Verwey, A., 1976. *Practical aspects of computational river hydraulics*, Pitman, London.
- De Roo, A.P.J., Price, D.A., Schmuck, G., 1999. Simulating the Meuse and Oder floods using the LISFLOOD model. In: Doel, P., Fohrer, N. (Eds.), *Modellierung des Wasser- und Stofftransports in grossen Einzugsgebieten. Proceedings of the Giessen Meeting*, November, Kassel University Press, 41–50.
- De Roo, A., Van Der Knijff, J., Horritt, M., Schmuck, G., De Jong, S., 1999. Assessing flood damages of the Oder flood and the Meuse flood. In: *Proceedings of the 2nd International Symposium on Operationalization of Remote Sensing*, Enschede, The Netherlands, 16–20 August. *Proceedings on CD-ROM*.
- Ervine, D.A., MacCleod, 1999. Modelling a river channel with distant floodbanks. *Proceedings of the Institution of Civil Engineers, Water Maritime and Energy* 136, 21–33.
- Ervine, D.A., Willets, B.B., Sellin, R.H.J., Lorena, M., 1993. Factors affecting conveyance in meandering compound flows. *Journal of Hydraulic Engineering American Society of Civil Engineers* 119, 1383–1399.
- Ervine, D.A., Sellin, R.H.J., Willets, B.B., 1994. Large flow structures in meandering compound channels. In: White, W.R., Watts, J. (Eds.). *Proceedings of the 2nd International Conference on River Flood Hydraulics*, Wiley, pp. 459–470.
- Estrela, T., 1994. Use of a GIS in the modelling of flows on floodplains. In: White, W.R., Watts, J. (Eds.). *Proceedings of the 2nd International Conference on River Flood Hydraulics*, Wiley, pp. 177–189.
- Feldhaus, R., Höttges, R., Brockhaus, T., Rouvé, G., 1992. Finite element simulation of flow and pollution transport applied to part of the River Rhine. In: Falconer, R.A., Shiono, K., Matthews, R.G.S. (Eds.). *Hydraulic and Environmental Modelling: Estuarine and River Waters*, Ashgate, Aldershot, pp. 323–334.
- Fread, D.L., 1984. In: Anderson, M.G., Burt, T.P. (Eds.). *Hydrological Forecasting*, Wiley, Chichester (chap. 14).
- Fread, D.L., 1993. In: Maidment, D.R. (Ed.). *Handbook of Applied Hydrology*, McGraw-Hill, New York (chap. 10).
- Horritt, M.S., 1999. A statistical active contour model for SAR image segmentation. *Image and Vision Computing* 17, 213–224.
- Imhoff, M.L., Vermillion, C., Story, M.H., Choudhury, A.M., Gafoor, A., Polcyn, F., 1997. Monsoon flood boundary delineation and damage assessment using space borne imaging radar and Landsat data. *Photogrammetric Engineering and Remote Sensing* 54, 405–413.
- Knight, D.W., Shiono, K., 1996. River channel and floodplain hydraulics. In: Anderson, M.G., Walling, D.E., Bates, P.D. (Eds.). *Floodplain Processes*, Wiley, Chichester, pp. 139–182.
- Li, C.S., 1997. Waveform sampling LiDAR applications in complex terrain. *International Journal of Remote Sensing* 18, 2087–2104.

- Marks, K., Bates, P.D., 2000. Integration of high-resolution topographic data with floodplain flow models. *Hydrological Processes* (in press).
- Penning-Rowsell, E.C., Tunstall, S.M., 1996. Risks and resources: defining and managing the floodplain. In: Anderson, M.G., Walling, D.E., Bates, P.D. (Eds.). *Floodplain Processes*, Wiley, Chichester, pp. 493–533.
- Priestnall, G., Jaafar, J., Duncan, A., 2000. Extracting urban features from LiDAR-derived digital surface models. *Computers, Environment and Urban Systems* (in press).
- Romanowicz, R., Beven, K.J., Tawn, J., 1996. Bayesian calibration of flood inundation models. In: Anderson, M.G., Walling, D.E., Bates, P.D. (Eds.). *Floodplain Processes*, Wiley, Chichester, pp. 333–360.
- Samuels, P.G., 1990. Cross section location in one-dimensional models. In: White, W.R. (Ed.). *International Conference on River Flood Hydraulics*, Wiley, Chichester, pp. 339–350.
- Sellin, R.H.J., Willets, B.B., 1996. Three-dimensional structures, memory and energy dissipation in meandering compound channel flow. In: Anderson, M.G., Walling, D.E., Bates, P.D. (Eds.). *Floodplain Processes*, Wiley, Chichester, pp. 255–298.
- Singh, V.P., 1996. *Kinematic wave modelling in water resources: surface water hydrology*, Wiley, New York (1399 pp.).
- Tholey, N., 1995. Monitoring flood events with remote sensing data: an example of ERS-1's contribution to flood events in Northern and Southern France regions. In: *Proceedings of the 1st ERS Thematic Working Group Meeting on Flood Monitoring*, ESA-ESRIN, Frascati, Italy.
- Thomas, T.G., Williams, J.J.R., 1995. Large eddy simulation of turbulent flow in an asymmetric compound open channel. *Journal of Hydraulic Research* 33, 27–41.
- Tominaga, A., Nezu, I., 1991. Turbulent flow structure in compound channel flows. *Journal of Hydraulic Engineering*, American Society of Civil Engineers 117, 21–41.
- Van Deursen, W.P.A., Wesseling, C.G., 1996. *PCRaster version 2 manual*. Department of Physical Geography, Utrecht University, The Netherlands.
- Wesseling, C.G., Karssenbergh, D.J., Burrough, P.A., Van Deursen, W.P.A., 1996. Integrating dynamic environmental models in GIS: the development of a dynamic modelling language. *Transactions in GIS* 1-1, 40–48.
- Younis, B.A., 1996. Progress in turbulence modelling for open channel flows. In: Anderson, M.G., Walling, D.E., Bates, P.D. (Eds.). *Floodplain Processes*, Wiley, Chichester, pp. 299–332.